Metaclusters for the Full Control of Mechanical Waves

Pawel Packo,[1] Andrew N. Norris,[2] and Dani Torrent[3,*]

[1] *Department of Robotics and Mechatronics, AGH - University of Science and Technology, Al. A. Mickiewicza 30, Krakow 30-059, Poland*

[2] *Mechanical and Aerospace Engineering, Rutgers University, Piscataway, New Jersey 08854-8058, USA*

[3] *GROC, UJI, Institut de Noves Tecnologies de la Imatge (INIT), Universitat Jaume I, Castelló 12071, Spain*

(Received 28 September 2020; revised 7 December 2020; accepted 23 December 2020; published 27 January 2021)

We present a method for the control of waves based on inverse multiple scattering theory. Conceived as a generalization of the concept of metagrating, we call metaclusters to a finite set of scatterers whose position and properties are obtained by inverse design once we have defined their response to some external incident field. The particular focus is on designing passive metaclusters that do not require an external source of energy. The method is applied to the propagation of flexural waves in thin plates, and to the design of far-field patterns, although its generalization to acoustic or electromagnetic waves is straightforward. Numerical examples are presented to the design of uni- and bidirectional "anomalous scatterers," which will bend the scattering energy along a specific direction, "odd pole" scatterers, whose radiation pattern presents an odd number of poles, and to the generation of vortical patterns. Finally, some considerations about the optimal design of these metaclusters are discussed.

DOI: 10.1103/PhysRevApplied.15.014051

I. INTRODUCTION

Active and passive control of the energy transfer in electromagnetic and mechanical waves is a challenging problem with a large number of applications, such as focusing, imaging, beam forming, cloaking and energy harvesting, among others [1]. The advent of so-called metamaterials [2,3] provided a different perspective since these artificial structures allow the design of materials with extraordinary properties capable of manipulating the flow of energy in ways that would be impossible with common materials, enlarging in this manner the number of devices for the control of electromagnetic and mechanical waves.

More recently, the concept of "metasurface," conceived as artificial planar metamaterials, has attracted an increasing interest. Being thinner and less dissipative than bulk metamaterials, these structures allow for more efficient ways of manipulating the wave energy, with the additional simplification in fabrication that planar structures present in comparison with bulk structures [4–6].

The major drawback of both metamaterials and metasurfaces however is that their functionality is based on the extraordinary refractive and reflective properties they present, and most of the devices designed in this framework require a large number of scattering elements in order to form an "effective" material whose effective physical properties provide metamaterials of their extraordinary properties. In the case of metasurfaces, the surface has to be gradually structured so that the effective gradient in the surface impedance allows for the manipulation of the energy flow. This large number of scattering elements is an important limitation in the efficiency of metamaterials and metasurfaces, since in practice the number of different scattering elements will be limited, especially on the micro- or nanoscale.

To overcome these difficulties, several approaches have been explored recently to simplify the design of metasurfaces by means of diffraction gratings [7–12], in which it has been possible to find a complex scatterer or unit cell performing the same functionality as some metasurfaces. However, the design process is still complex and functionality is limited to the control of the propagation direction of waves [13–15].

In this work, we present a generalization of the concept of a metagrating but for finite structures. The objective is to show how, for a given incident field, we can obtain a cluster of scatterers and their physical properties such that the scattered field presents a preselected shape. If a particular diffraction pattern is desired for a specific type of incident wave, we provide a method to design a cluster of scatterers capable of transferring the energy along the desired directions. The inverse design method presented is based on multiple scattering theory [16] and the general principle is applicable to any kind of classical wave, including acoustic and electromagnetic waves. We use flexural waves in plates as the model medium, due to their potential wide

*dtorrent@uji.es

application, but the presented framework is general and applicable to wave scattering in other media. This work therefore provides a general principle for the full control of mechanical and electromagnetic waves based on scattering elements.

The paper is organized as follows. After this introduction, in Sec. II we develop the idea of the direct and inverse multiple scattering problem. In Sec. III we explain how the method can be applied to the design of far-field patterns and in Sec. IV we show numerical examples of specific patterns. Finally, in Sec. V we summarize the work and some mathematical results are given in Appendices A and B.

II. DIRECT AND INVERSE MULTIPLE SCATTERING PROBLEM

When some incident field ψ_0 impinges on a cluster of N pointlike scatterers, the total field $\psi(\mathbf{r})$ can be expressed as the sum of the incident plus the scattered fields,

$$\psi(\mathbf{r}) = \psi_0(\mathbf{r}) + \psi_s(\mathbf{r}). \tag{1}$$

The scattered field is

$$\psi_s(\mathbf{r}) = \sum_{\beta=1}^{N} B_\beta G(\mathbf{r} - \mathbf{R}_\beta), \tag{2}$$

where $G(\mathbf{r}) = G(|\mathbf{r}|)$ is Green's function and the coefficients B_β are obtained from the multiple scattering equation [17]

$$\sum_{\beta=1}^{N} [t_\beta^{-1}\delta_{\alpha\beta} - G(\mathbf{R}_\alpha - \mathbf{R}_\beta)]B_\beta = \psi_0(\mathbf{R}_\alpha). \tag{3}$$

This provides a system of N equations with N unknowns. The quantity t_α is the strength of each pointlike scatterer and it is the only quantity that contains information about its physical properties. This describes the direct multiple scattering problem, in which the number of scatterers, N, their strengths t_α, and locations $\mathbf{R}_\beta$ are known, from which we compute the B_α coefficients to finally determine the field in all of space.

The inverse problem is as follows. Assume that the scattered field can be expressed as a linear combination of basis functions ϕ_n such that

$$\psi_s(\mathbf{r}) = \sum_{n=-\infty}^{\infty} A_n \phi_n(\mathbf{r}). \tag{4}$$

Then we specify the inverse problem as determining a finite number N_p of A_n coefficients for $n = 1, \ldots, N_p$, so that the scattered field will have a specified radiation pattern in the far field. In general, there will be a matrix S such that

$$A_n = \sum_{\beta=1}^{N} S_{n\beta} B_\beta; \tag{5}$$

therefore, if we select the number N of particles in the cluster equal to the number N_p of modes to design, Eq. (5) constitutes a determinate system of N equations with N unknowns from which we can solve for the B_β coefficients. Once these are known, we can obtain the t_α elements from Eq. (4) as

$$t_\alpha^{-1} = \frac{1}{B_\alpha}\left(\psi_0(\mathbf{R}_\alpha) + \sum_{\beta=1}^{N} G(\mathbf{R}_\alpha - \mathbf{R}_\beta)B_\beta\right). \tag{6}$$

Thus, we can obtain the physical properties of each particle. The main challenge is to find a cluster configuration giving physically acceptable particles.

For the case of flexural waves on thin elastic plates, ψ is the plate deflection, G is the solution for a point force per unit area applied in the positive ψ direction, and

$$B_\alpha = t_\alpha \psi(\mathbf{R}_\alpha) \tag{7}$$

is the point force per unit area of scatterer α; see Appendix A. The parameter t_α is an effective point impedance that can be interpreted in terms of a single-degree-of-freedom system with mass, stiffness, and damping. Physically acceptable particles cannot supply energy, i.e., they must be passive. Assuming time dependence $e^{-i\omega t}$, the passivity constraints require that one or other of the following conditions is met:

$$\sum_{\alpha=1}^{N} (\operatorname{Im} t_\alpha^{-1})|B_\alpha|^2 \le 0, \tag{8a}$$

$$\operatorname{Im} t_\alpha^{-1} \le 0. \tag{8b}$$

Equation (8a) requires that the cluster be globally passive, meaning that some of the scatterers can provide energy, but there should be a negative energy balance adding all the contributions of the scatterers. Equation (8b), or equivalently $\operatorname{Im} t_\alpha \ge 0$, is a more restrictive condition, since it requires that all scatterers be passive systems (see Appendix A for details). The equality holds for zero dissipation in both equations. The goal of the inverse multiple scattering problem is to obtain a set of particles all simultaneously satisfying the first constraint or both constraints. For the first constraint, global passivity, we assume that, although some scatterers may require energy supply, this energy can be transferred from other, locally passive ones (see Appendix A).

The specific problem addressed below is to engineer the cluster of point scatterers to provide a close approximation to a desired far-field scattering response. In the next section we outline the steps necessary to achieve this in an optimal sense.

III. FAR-FIELD ENGINEERING

A. Direct far-field solution

The functions ϕ_n of Eq. (4) are chosen as the infinite set

$$\phi_n(\mathbf{r}) = G(\mathbf{r})e^{in\theta}, \qquad n \in \mathbb{Z}, \tag{9}$$

where the position is expressed in polar coordinates $\mathbf{r} = (r,\theta)$ with respect to an origin at $r = 0$. This allows us to uniquely identify the coefficients A_n of Eq. (4) as far-field amplitudes of the scattered wave. In order to see this, first note that the far field for a source at $\mathbf{R}_\beta = (R_\beta,\theta_\beta)$ is

$$G(\mathbf{r} - \mathbf{R}_\beta) \approx G(\mathbf{r})e^{-ikR_\beta\cos(\theta-\theta_\beta)}. \tag{10}$$

This approximation holds whether Green's function is for the Helmholtz equation or for the Kirchhoff plate equation. In both cases, the far-field response depends only on the large argument approximation of $H_0^{(1)}(x)$. The scattered far field of the cluster follows from Eqs. (2) and (10) as

$$\psi_s(\mathbf{r}) \approx G(\mathbf{r})f(\theta), \tag{11}$$

with the far-field radiation function

$$f(\theta) = \sum_{\beta=1}^{N} B_\beta e^{-ikR_\beta\cos(\theta-\theta_\beta)}. \tag{12}$$

Alternatively,

$$f(\theta) = \sum_{n=-\infty}^{\infty} A_n e^{in\theta}, \tag{13}$$

where the infinite set of coefficients $\{A_n\}$ is related to the N coefficients $\{B_\beta\}$ by Eq. (5) with

$$S_{n\beta} = (-i)^n e^{-in\theta_\beta} J_n(kR_\beta). \tag{14}$$

For a unit amplitude incident plane wave propagating in the direction $\theta = 0$, the radiation pattern function satisfies the optical theorem [18]

$$\mathrm{Im} f(0) = \sigma_{\mathrm{sca}} + \sigma_{\mathrm{abs}}, \tag{15}$$

where the scattering cross section σ_{sca} and absorption cross section σ_{abs} are defined in Eqs. (A6b) and (A6c). Further details can be found in Appendix A. The cross sections can also be expressed directly in terms of the coefficients $\{A_n\}$ and $\{B_\beta\}$ [see Eq. (A8)], leading to the explicit form of the optical theorem

$$\mathrm{Im} f(0) = \frac{1}{8Dk^2}\mathbf{A}^\dagger\mathbf{A} + \sum_{\alpha=1}^{N}(-\mathrm{Im}\, t_\alpha^{-1})|B_\alpha|^2. \tag{16}$$

We define the energy efficiency of a cluster as the ratio of scattered to total input energy, which can be calculated from the scattering and absorption cross sections of Eqs. (A6) as

$$\eta = \frac{\sigma_{\mathrm{sca}}}{\sigma_{\mathrm{ext}}} = \frac{\sigma_{\mathrm{sca}}}{\sigma_{\mathrm{sca}} + \sigma_{\mathrm{abs}}}. \tag{17}$$

B. Inverse problem

In the inverse source problem we are given $f(\theta)$ and seek the cluster that optimally reproduces this scattering pattern. The radiation pattern, defined by the coefficients $\{A_n\}$ in the form (13), is infinite dimensional, whereas the cluster comprises a finite set of N sources. We define the error

$$\begin{aligned} E &= \int_0^{2\pi} \left| \sum_{n=-\infty}^{\infty} \left(A_n - \sum_{\beta=1}^{N} S_{n\beta}B_\beta \right) e^{in\theta} \right|^2 \\ &= \|\mathbf{A} - \mathbf{SB}\|^2, \end{aligned} \tag{18}$$

where $\|\mathbf{X}\|^2 = \mathbf{X}^\dagger\mathbf{X}$ with $\mathbf{X}^\dagger$ the Hermitian transpose of vector $\mathbf{X}$. Minimizing E for given $\mathbf{A}$ and $\mathbf{S}$ yields the solution

$$\mathbf{B} = (\mathbf{S}^\dagger\mathbf{S})^{-1}\mathbf{S}^\dagger\mathbf{A}, \tag{19}$$

where $(\mathbf{S}^\dagger\mathbf{S})^{-1}\mathbf{S}^\dagger$ may be identified as the Moore-Penrose inverse of $\mathbf{S}$.

The approximated radiation pattern is

$$f^{(N)}(\theta) = \sum_{n=-\infty}^{\infty} A_n^{(N)} e^{in\theta}, \tag{20}$$

where $A_n^{(N)}$, $n \in \mathbb{Z}$, are the elements of

$$\mathbf{A}^{(N)} = \mathbf{SB} = \mathbf{PA}, \tag{21}$$

and the non-negative definite Hermitian matrix $\mathbf{P}$ is

$$\mathbf{P} = \mathbf{S}(\mathbf{S}^\dagger\mathbf{S})^{-1}\mathbf{S}^\dagger. \tag{22}$$

We show in Appendix B that the matrix $\mathbf{P}$ is infinite dimensional but finite rank with N nonzero eigenvalues equal to $+1$; see Eq. (B5). It therefore acts as a projection from the infinite-dimensional space of far-field pattern functions to

the N-dimensional set of approximate pattern functions: $f(\theta) \to f^{(N)}(\theta)$.

The optimal solution (21) yields an error

$$E = \mathbf{A}^\dagger(\mathbf{A} - \mathbf{A}^{(N)}) = \|\mathbf{A}\|^2 - \|\mathbf{QA}\|^2, \tag{23}$$

where

$$\mathbf{Q} = (\mathbf{S}^\dagger\mathbf{S})^{-1/2}\mathbf{S}^\dagger. \tag{24}$$

In practice, we are interested in the relative error $E_{\rm rel} = E/\|\mathbf{A}\|^2$, i.e.,

$$E_{\rm rel} = 1 - \frac{\mathbf{A}^\dagger\mathbf{A}^{(N)}}{\|\mathbf{A}\|^2}. \tag{25}$$

1. Invisibility?

Can the cluster be invisible, in the sense that there is no scattered wave? Setting $\mathbf{A}$ to zero implies that

$$0 = \mathbf{SB} \quad \Longrightarrow \quad \mathbf{S}^\dagger\mathbf{SB} = 0. \tag{26}$$

Hence, $B_\alpha = 0$, and therefore $t_\alpha = 0$, meaning that there are no scatterers, the null solution. We conclude that the inverse scattering cluster scheme does not provide a useful route to invisibility or cloaking.

C. Inverse design algorithm

Based on the above findings, the inverse scattering design can be formulated as follows.

(1) The N scatterer positions $\mathbf{R}_\alpha$, $\alpha = 1, \ldots, N$, are defined.

(2) The desired far-field pattern $f(\theta)$ is specified, or, equivalently, the set of far-field modal amplitudes $\{A_n,\ n \in \mathbb{Z}\}$ are given [see Eq. (13)].

(3) The frequency (equivalently the wave number k) is given.

(4) The matrices $\mathbf{S}$ and $\mathbf{P}$ are evaluated [see Eqs. (14) and (22)].

(5) The source strengths B_α, the optimal approximation to the far-field pattern $f^{(N)}(\theta)$, i.e., $\{A_n^{(N)},\ n \in \mathbb{Z}\}$, and the relative error $E_{\rm rel}$ are calculated [see Eqs. (13), (19), and (25)].

(6) An incident wave field $\psi_0(\mathbf{r})$ is defined, and the particle impedances t_α, $\alpha = 1, \ldots, N$, are calculated [see Eq. (6)].

The first two items are geometrical, independent of frequency and the incident wave. Once the frequency is defined, the approximation $f^{(N)}(\theta)$ to the scattered far field is optimal in the sense of an N-dimensional solution according to the setup, and it is independent of the incident field. The form of the incident wave, combined with the source amplitudes B_α, defines the required particle impedances t_α in Eq. (6).

The inverse algorithm defines the mechanical properties of the configuration, i.e., the t_α, for a given incident wave ψ_0. If the incident wave changes then the new scattering coefficients B_α are defined by the system of equations (3) with the predetermined $\{t_\alpha\}$. Regardless of the incident wave direction, the process remains reciprocal under the interchange of incident and scattering directions.

The question that must be addressed is whether or not all of the scatterer impedances satisfy the passivity constraints (8a) or (8b).

IV. APPLICATIONS

A. Far-field patterns and the matrix P

Two groups of cluster patterns are considered, namely regular polygons, where scatterers are uniformly distributed over a circle, and finite lattices, where scatterers are regularly distributed in a two-dimensional finite grid. We describe how different arrangements of the scatterers influence the matrix $\mathbf{P}$ of Eq. (22) that defines the optimal approximation to the desired scattering pattern.

1. Scatterers on a regular polygon

Let us assume that the N scatterers lie on the circle of radius R at $\theta_\beta = 2\pi\beta/N$. We consider $\mathbf{A}$ corresponding to each of the modes $e^{im\theta}$, $m \in \mathbb{Z}$, so that $\|\mathbf{A}\|^2 = 1$ and $E \le 1$ with $E \ll 1$ indicating that the desired scattering mode is well approximated. The results of numerical experimentation are as follows. For small kR relative to N, E is small for modes $m = 0, \pm 1, \ldots, (N-1/2)$ if $N > 1$ is odd and for modes $m = 0, \pm 1, \ldots, (N-2/2)$ if N is even, with $E \approx 0.5$ for $m = \pm(N/2)$. The accuracy diminishes as kR increases. In other words, for small kR, the N unit eigenvalues of $\mathbf{P}$ correspond to modes $m = 0, \pm 1, \ldots, (N-1/2)$ if $N > 1$ is odd, with analogous association for N even. Since the modes are multiply degenerate (all of eigenvalue unity), it follows that any linear combination of these modes is an eigenvector.

2. Scatterers on a finite square lattice

We now assume that the scatterers are distributed in a square but finite lattice. The lattice is $M \times M \equiv N$ with lattice spacing a. For instance, with $M = 3$ and $ka = 1$, we find that the nine eigenvectors of $\mathbf{P}$ of eigenvalue $+1$ span the space $\Omega_4 \equiv \{e^{im\theta},\ m = 0, \pm 1, \ldots, \pm 4\}$. This result is arrived at by inspecting the error E for each mode, and noting that it is small, of the order of 1×10^{-4} typically, while higher modes have error of approximately unity. However, for the same $ka = 1$ but the larger lattice with $M = 4$ $(N = 16)$, we find that the nontrivial eigenspace is $\Omega_5 \cup \Omega_{6,10}$, where $\Omega_{6,10}$ is a five-dimensional subspace formed from $\{e^{im\theta},\ m = \pm 6, \ldots, \pm 10\}$.

3. General properties of the P matrix

Numerical experiments on matrix **P** for different spatial configurations of the clusters show that, for large and moderate kR, there are exactly N eigenvalues of **P** with values close to 1. For large kR, the corresponding eigenvectors (i.e., patterns of scattering modes of the cluster) are highly irregular and sensitive to both kR and scatterer positions (while the number of eigenvalues of value 1 equals N). For $kR_c \approx 0.5$ and smaller, where R_c is the characteristic size of the cluster, the eigenvalues of **P** begin to differ and assume values other than 1. For $kR_c \ll 1$, the number of nonzero eigenvalues reduces and low-order scattering patterns are preferred.

Some general remarks on the number of scatterers (N) and scattering properties of the cluster can be formulated as follows. The larger N, the larger the number of cluster modes; thus, more complex scattering patterns can be reproduced accurately. Large number of scatterers in the cluster, on the other hand, may result in overconstraining the minimization problem and a lack of locally or globally passive solutions. For moderate kR_c, typically the number of regular patterns (eigenvectors of **P**) is similar to N, while more degenerate patterns and/or a smaller number of similar eigenvalues (approximately 1) are observed for large or small kR_c.

B. Scattering patterns

The inverse design of metaclusters is illustrated with the scatterers arranged on regular polygons or square lattices, as outlined in Sec. IV A. Here we present the target scattering patterns that will be later reproduced by proper selection of passive impedances.

1. Uni- and bidirectional scattering patterns

Unidirectional scattering in the direction $\theta = \theta_0$ corresponds to

$$f(\theta) = C_0\delta(\theta-\theta_0) \quad \Longleftrightarrow \quad A_n = \frac{C_0}{2\pi}e^{-in\theta_0}. \tag{27}$$

A bidirectional scattering pattern is of the form $f(\theta) = C_0\delta(\theta-\theta_0) + C_1\delta(\theta-\theta_1)$. We consider patterns that are symmetric or antisymmetric about the x direction ($\theta = 0$), corresponding to $\theta_1 = -\theta_0$ and $C_1 = \pm C_0$. We may choose $C_0 = 1$ with no loss in generality, and define

$$f_\pm(\theta,\theta_0) \equiv \delta(\theta-\theta_0) \pm \delta(\theta+\theta_0)$$
$$\Longleftrightarrow \quad A_n = \begin{cases} \dfrac{1}{\pi}\cos n\theta_0, \\ -\dfrac{i}{\pi}\sin n\theta_0. \end{cases} \tag{28}$$

Examples of the uni- and bidirectional scattering patterns are shown in Figs. 1(a) and 1(b).

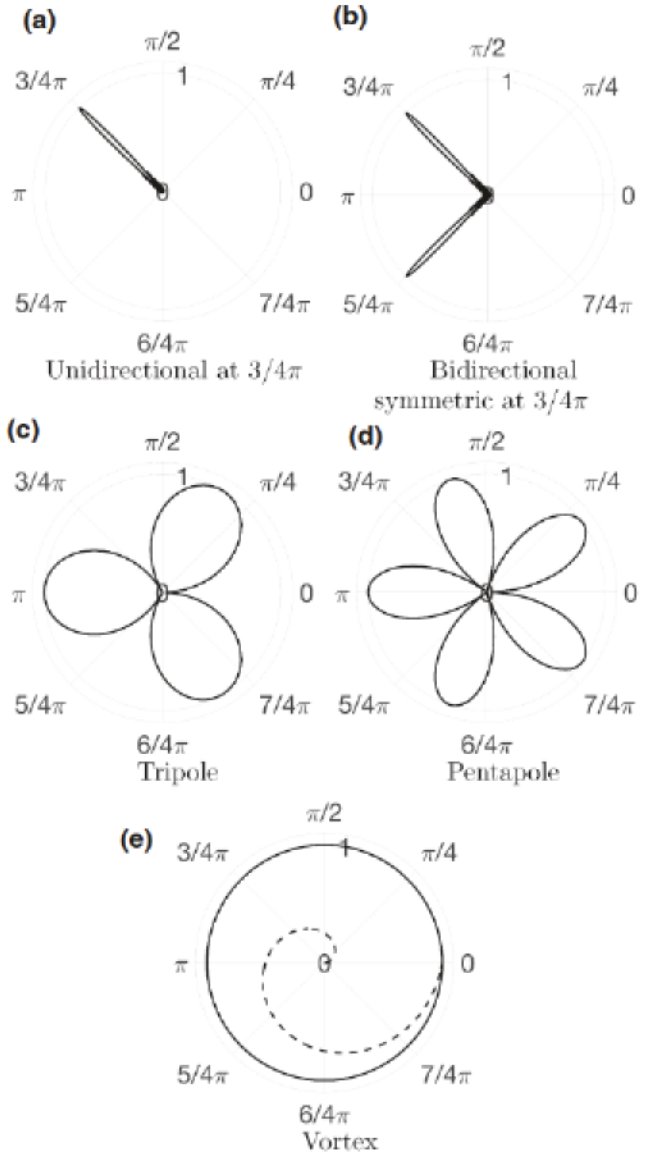

FIG. 1. Examples of the target patterns. Solid lines are normalized amplitudes, and dashed lines are normalized phases of the pattern functions (a finite number of 81 modes in Eq. (13) is assumed).

2. Odd-pole patterns

Odd-pole patterns have $\bar{p}$ scattering lobes directing energy towards the preferential directions. The odd-pole scattering pattern and the corresponding A_n coefficients are given as

$$f(\theta) = \sin\left(\frac{\bar{p}}{2}\theta'\right) \quad \Longleftrightarrow \quad A_n = \frac{\bar{p}\sin^2(\bar{p}/2+n)(\pi/2)}{\pi[(\bar{p}/2)^2-n^2]}, \tag{29}$$

where $\theta' = \theta \bmod 2\pi$ is used to ensure that $f(\theta)$ is a 2π-periodic function.

a. A tripole. For a tripolar pattern, $\bar{p} = 3$, there are three main lobes spaced every $2/3\pi$. An example of a tripolar pattern is shown in Fig. 1(c).

b. A pentapole. Similarly, for $\bar{p} = 5$, a pentapole scattering pattern is obtained. See Fig. 1(d) for this type of pattern.

3. A vortex

A vortex generates a uniform constant amplitude pattern with angle-dependent linearly changing phase behavior. The corresponding formulas for the vortex of order $\bar{p} \in \mathbb{Z}$ are

$$f(\theta) = e^{i\bar{p}\theta} \quad \Longleftrightarrow \quad A_n = \delta_{n\bar{p}}. \tag{30}$$

Directional characteristics of amplitudes and phases for the vortex pattern are shown in Fig. 1(e).

C. Full metacluster designs

Designing a metacluster requires finding all t_α for a given cluster topology and the desired scattering pattern. The procedure outlined in Sec. III C is employed here to find t_α. We first present metacluster scattering patterns corresponding to the desired patterns from Sec. IV B, obtained for different clusters configurations. Since the inverse procedure frequently leads to active particles, we next impose condition (8b) to find locally passive optimal metaclusters and present their scattering responses. For all presented examples, we introduce the incident wave—without loss of generality—assumed to be a plane wave in the $-x$ direction ($\theta = \pi$).

1. Scattering patterns for optimal metaclusters

Scattering patterns obtained for selected cluster topologies are shown in Fig. 2. Very good agreement between the desired patterns of Fig. 1 can be seen, proving the effectiveness of the design procedure. However, some of the corresponding impedances—computed using the inverse approach of Sec. III C—are active and hence require energy supply. We next analyze and adopt the inverse procedure for seeking only locally passive solutions.

2. An optimization problem for passive metaclusters

Our design objective is the set of point impedances $\{t_\alpha, \alpha = 1, \ldots, N\}$. We aim at fulfilling the local passivity condition, Eq. (8b). Define

$$u_\alpha = t_\alpha^{-1}, \tag{31a}$$

$$p_\alpha = B_\alpha^{-1}\psi_0(\mathbf{R}_\alpha), \tag{31b}$$

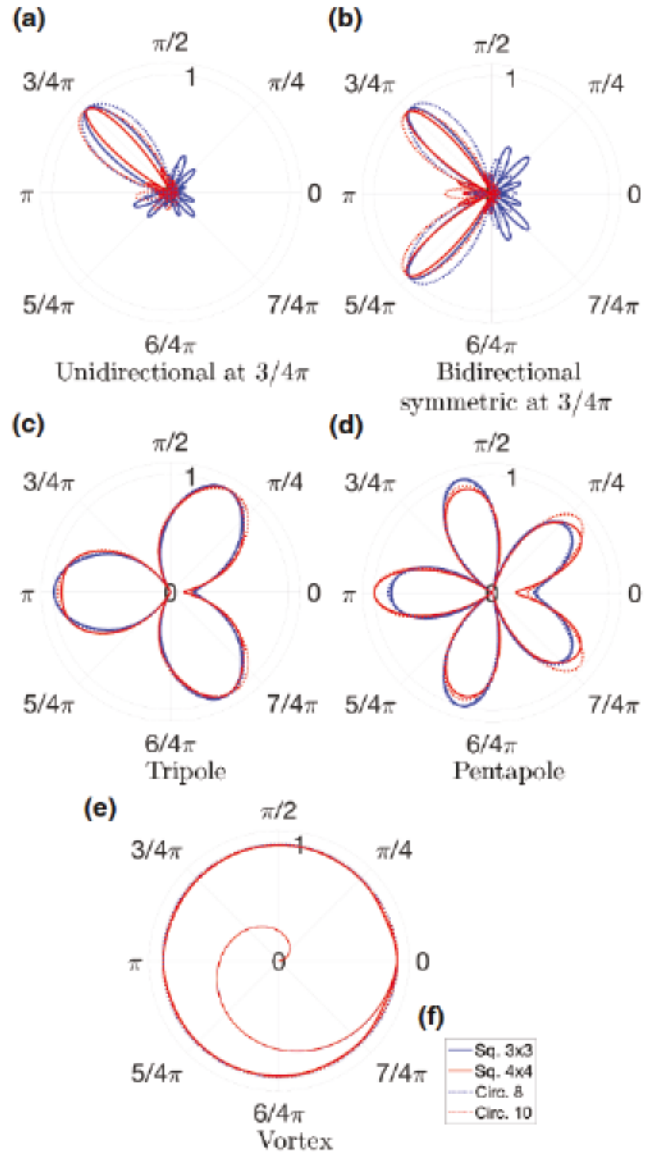

FIG. 2. Examples of the optimal far-field patterns for square 3×3 and 4×4 arrays (lattice spacing a) and circular arrangements with 8 and 10 particles (radius a) for $ka = 1$ based on Eqs. (20) and (21). Incidence angle $\theta = \pi$ (the $-x$ direction). For the vortex, Fig. 2(e), circular shapes are amplitude profiles while the spirals in the center are phases of the scattering pattern. All patterns are normalized.

$$s_\alpha = B_\alpha^{-1} \sum_{\beta=1}^{N} G(\mathbf{R}_\alpha - \mathbf{R}_\beta) B_\beta. \tag{31c}$$

Then Eq. (6) becomes $u_\alpha = p_\alpha + s_\alpha$, $\alpha = 1, \ldots, N$. Consider plane-wave incidence $\psi_0(\mathbf{r}) = p_0 e^{i\mathbf{k}\cdot\mathbf{r}}$ for some wave number $\mathbf{k}$. There is a further degree of freedom that has not been used. This could be considered as the amplitude and phase of the incident wave, i.e., the complex number p_0. Alternatively, if we fix $p_0 = 1$ then there is a similar

degree of freedom in how we normalize the far-field pattern function $f(\theta)$. This has the effect of scaling $\mathbf{A}$ and hence $\mathbf{B}$ by a complex number. This scaling redefines p_α but has no effect on s_α of Eq. (31c). Therefore, with no loss in generality, we assume that the incident wave has unit amplitude,

$$\psi_0(\mathbf{r}) = e^{i\mathbf{k}\cdot\mathbf{r}}, \tag{32}$$

and rewrite Eq. (6), the solution of the inverse problem, to incorporate this added degree of freedom, as

$$u_\alpha = zp_\alpha + s_\alpha, \qquad \alpha = 1, \ldots, N. \tag{33}$$

Here the complex number z defines the scaling of the pattern function, which goes as z^{-1}. The important point is that z can be chosen arbitrarily; in particular, we use it as an optimization parameter. The fact that the pattern function amplitude is inversely proportional to $|z|$ for a unit amplitude incident wave suggests that smaller $|z|$ is preferred for maximizing the efficiency of energy conversion.

The optimization problem is as follows: given the N complex numbers p_α associated with the incident wave and the N complex numbers s_α associated with the point sources, find z of Eq. (33) that ensures that $\mathrm{Im}\, u_\alpha \le 0$ for all α. If this can be achieved then the optimal solution is the one with the minimum value of $|z|$, ensuring maximum amplitude for the pattern function. It might not be possible using the single complex number z to obtain all of the complex numbers u_α in the negative imaginary half-plane. If this is not achievable in practical examples then the constraint may be relaxed, for instance, to minimize the maximum instance of positive $\mathrm{Im}\, u_\alpha$. Then the "nearest" passive configuration can be identified by setting $\mathrm{Im}\, u_\alpha$ to zero for those particles with positive $\mathrm{Im}\, u_\alpha$. Another alternative could be based on condition (8a), i.e., when the metacluster is globally passive, meaning that the net energy supplied to the cluster is nonpositive.

In cases where the search procedure for t_α failed to find locally passive metaclusters, a rigid rotation is applied to the cluster (equivalent to changing the incidence angle) and the search is repeated.

3. Example: a passive optimal metacluster for uni- and bidirectional patterns

Numerical experimentation shows that there are metacluster configurations for which the inverse impedance solutions are all passive. Examples of the uni- and bidirectional scattering patterns for a square lattice metacluster are shown in Fig. 2. More detailed investigations show that, for instance, a square array with lattice parameter a designed to direct a wave incident from the $\theta = \pi$ direction into a scattered wave preferentially directed toward $\theta = 3/4\pi$ has totally passive solutions for $1.9 \le ka \le 2.8$.

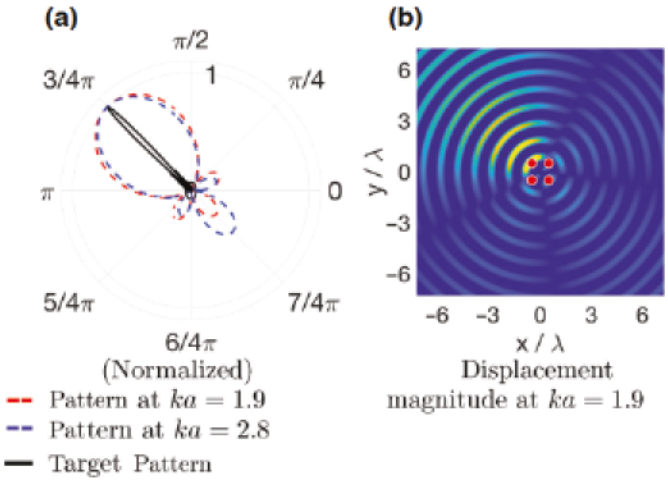

FIG. 3. The optimal pattern functions for the passive 2×2 metacluster at two frequencies bounding a bandwidth of passive designs, $ka \in \{1.9, 2.8\}$ (a), and the corresponding displacement field generated at $ka = 1.9$ (b). Admittances of the cluster are give in Table I. The efficiencies of the energy conversions are $\eta_{ka=1.9} = 0.60$ and $\eta_{ka=2.8} = 0.35$.

The optimal passive admittances t_α^{-1} are frequency dependent, with values at the end of the passive interval shown in Table I. The associated optimal scattering patterns are shown in Fig. 3. In all examples we take $a = 1$ and $D = 1$.

The examples in Fig. 3 and Table I are based on the value of z in Eq. (33) for which the largest value of $\mathrm{Im}\, t_\alpha^{-1}$ is zero. This optimizes the passive array in terms of its efficiency in converting the incident energy into a directed far-field pattern. The metacluster dissipates wave energy but in a way that is most efficient among all passive options. For the cluster shown in Fig. 3, the values of the efficiency parameter η of Eq. (17) are $\eta_{ka=1.9} = 0.60$ and $\eta_{ka=2.8} = 0.35$.

Similarly, in Fig. 4 we show a passive optimal 2×2 metacluster that converts the incident plane wave into a symmetric bidirectional pattern. Although the metacluster scattering pattern roughly approximates the desired far-field function, all admittances are purely real, indicating no dissipation in the system. Consequently, the energy efficiency for this cluster is optimal, $\eta = 1$.

TABLE I. The admittances t_α^{-1} for the 2×2 array of passive particles sending the wave incident at $\theta = \pi$ into the $\theta = 3/4\pi$ direction at two frequencies; see Fig. 3.

	t_α^{-1}	
$\mathbf{R}_\alpha$	$ka = 1.9$	$ka = 2.8$
$(-0.50, -0.50)$	$0.0662 - 0.0050i$	$0.0438 - 0.0000i$
$(-0.50, 0.50)$	$-0.0243 - 0.0000i$	$0.0214 - 0.0618i$
$(0.50, -0.50)$	$0.1120 - 0.0000i$	$-0.0651 - 0.1138i$
$(0.50, 0.50)$	$-0.0413 - 0.0316i$	$-0.0524 - 0.0009i$

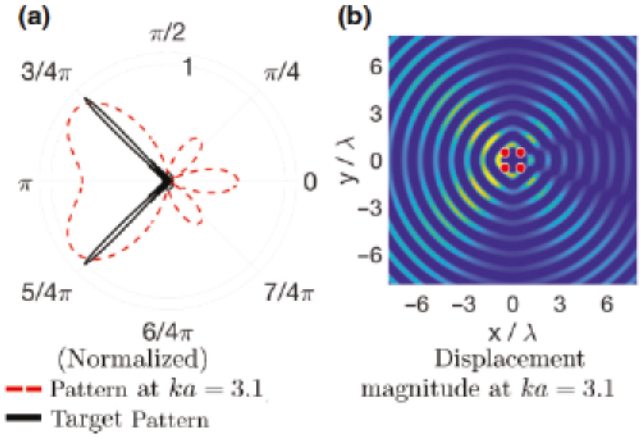

FIG. 4. The optimal pattern function for the passive 2×2 metacluster (a), and the corresponding displacement field generated at $ka = 3.1$ (b). Admittances of the cluster are given in Table II. The energy efficiency for this setup is $\eta = 1$.

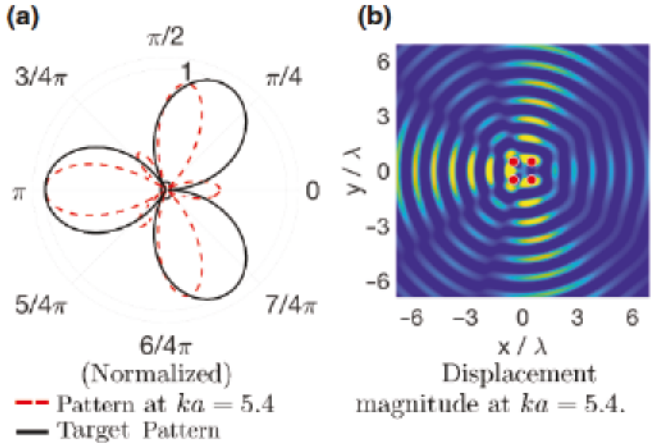

FIG. 5. The optimal pattern function for the passive 2×2 metacluster (a), and the corresponding displacement field generated at $ka = 5.4$ (b). Admittances of the cluster are give in Table III. The energy efficiency parameter is $\eta = 0.17$.

Further experimentation shows that the obtained optimal solutions are very sensitive to the scatterers' positions and impedances. Also, requirements of symmetric clusters are overconstrained, most often resulting in at least one active particle, especially for a large number of particles N.

4. Example: a passive optimal metacluster for odd-polar patterns

Analogously to the previous search, we look for optimal passive clusters capable of generating a scattering tripole. In Fig. 5 we show the target and the actual scattering patterns for the tripole obtained for a square 2×2 cluster of scatterers. The optimal positions and admittances of the scatterers are shown in Table III. The admittances have nearly the same passive damping properties. The corresponding displacement field pattern generated by the metacluster is shown in Fig. 5. The energy conversion efficiency is $\eta = 0.17$.

In Fig. 6 we show a metacluster designed for generating a pentapole pattern. The cluster consists of a circular arrangement of five scatterers with optimal positions and impedances listed in Table IV. Clearly, the cluster is locally passive. It is important to note that this metacluster setup, resulting in a nearly perfect pentapole [red dashed line in Fig. 6(a)], has been obtained accidentally when looking for the vortex-type scattering pattern [different than the pentapole pattern; see the black solid line in Fig. 6(a)]. The latter is a consequence of relaxing the requirement of enforcing the target phase of the scattered field and indicates that much more complex scattering patterns that are still locally passive may be obtained for desired amplitude-only rather than amplitude-and-phase target fields. This cluster also displays a high energy conversion efficiency of $\eta = 0.84$.

5. Example: a passive optimal metacluster for a vortex pattern

Finally, we present a locally passive metacluster capable of transforming the incident wavefield into the first-order vortex, $\bar{p} = 1$, as shown in Fig. 7. It can be seen from Fig. 7(a) that despite the fact that the amplitude pattern is not perfectly preserved, the phase behavior [Fig. 7(b)] recovers the linearly dependent angular characteristic of the vortex. In Figs. 7(c) and 7(d) we show displacements and phases of the wavefields generated by the metacluster. It is worth noting that this relatively complex scattering pattern is obtained by only four passive impedances.

TABLE II. The admittances t_α^{-1} for the 2×2 array of passive particles transforming the incident wave into a bidirectional symmetric pattern at $\theta = 3/4\pi$; see Fig. 4.

$\mathbf{R}_\alpha$	t_α^{-1} $(ka = 3.1)$
$(-0.50, -0.50)$	-0.0038
$(-0.50, 0.50)$	-0.0038
$(0.50, -0.50)$	-0.0111
$(0.50, 0.50)$	-0.0111

TABLE III. The admittances t_α^{-1} for the 2×2 array of passive particles sending the wave incident at $\theta = \pi$ for $ka = 5.4$ into the tripole pattern; see Fig. 5.

$\mathbf{R}_\alpha$	t_α^{-1} $(ka = 5.4)$
$(0.50, -0.50)$	$-0.0078 - 0.0211i$
$(-0.50, -0.50)$	$0.0029 - 0.0215i$
$(0.50, 0.50)$	$-0.0078 - 0.0211i$
$(-0.50, 0.50)$	$0.0029 - 0.0215i$

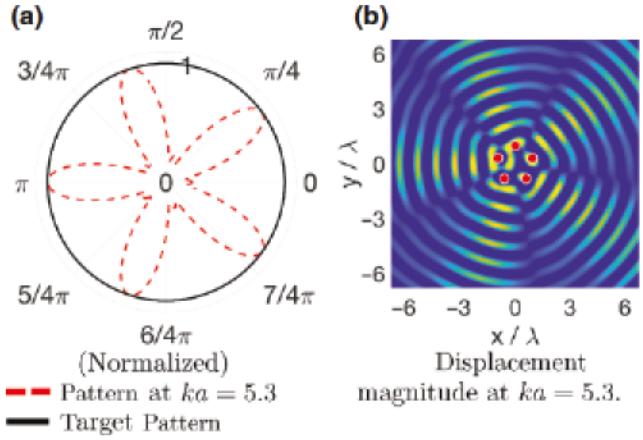

FIG. 6. The optimal pattern function for the passive circular metacluster of five particles (a), and the corresponding displacement field generated at $ka = 5.3$ (b). Admittances of the cluster are given in Table IV. The energy efficiency is $\eta = 0.84$ for this cluster configuration.

The cluster efficiency is $\eta = 0.14$ for this setup, being a consequence of moderate damping in all scatterers.

V. SUMMARY

We have shown that an inverse multiple scattering method can be applied for the design of the radiation patterns of clusters of scatterers. While the design process is complex and passive solutions are not easy to find, the approach has still more degrees of freedom to explore. The specific case of flexural waves in thin elastic plates has been considered, with the target problem of designing the far-field patterns, although it is easy to show that near-field patterns can also be considered. Similarly, the multiple scattering formulation is not unique to flexural waves, and the approach introduced here can be easily extended to other classical waves, like optical or acoustical. Further analysis using clusters of finite-size scatterers is important for physical realization of the directivity effect. While the analysis of such attachments requires introduction of scattering matrices for each object, the structure of the framework proposed here remains unchanged but becomes more involved. However, some simplifications can be made for low-frequency approximations of finite-size scatterers, reducing the infinite scattering matrix to only several terms describing monopoles, dipoles, etc. These issues are under current investigation, and we expect to report on the acoustic analog in the near future.

TABLE IV. The admittances t_α^{-1} for the five-element circular array of passive particles sending the wave incident at $\theta = \pi$ for $ka = 5.3$ into the pentapole pattern; see Fig. 6.

$\mathbf{R}_\alpha$	t_α^{-1} $(ka = 5.3)$
(0.95, 0.31)	$0.0007 - 0.0020i$
(0.00, 1.00)	$0.0009 - 0.0021i$
(−0.95, 0.31)	$0.0011 - 0.0020i$
(−0.59, −0.81)	$-0.0045 - 0.0002i$
(0.59, −0.81)	$0.0064 - 0.0003i$

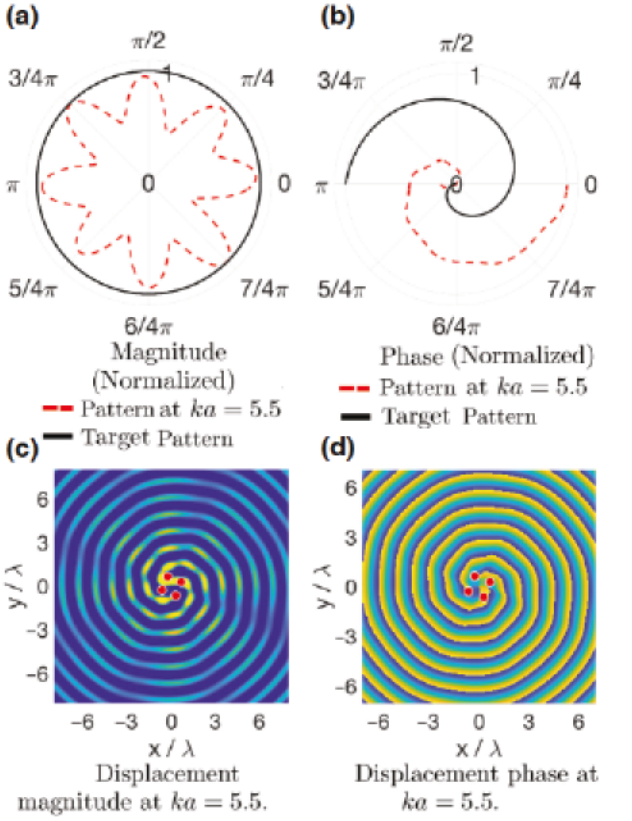

FIG. 7. The optimal pattern function for the passive 2×2 metacluster: amplitude (a) and phase (b); and the corresponding displacement field generated at $ka = 5.5$: displacement magnitude (c) and phase (d). Admittances of the cluster are given in Table V. The energy efficiency is $\eta = 0.14$.

The proposed metaclusters can be considered a generalization of the notion of a metagrating, where the inverse design is performed in the amplitude of the diffraction orders and the structures are periodic gratings. However, in contrast with the infinite number of scattering elements in a metagrating, the present results are based on clusters of very few scatterers. In light of the small number of

TABLE V. The admittances t_α^{-1} for the 2×2 square array of passive particles sending the wave incident at $\theta = \pi$ for $ka = 5.5$ into the vortex pattern; see Fig. 7.

$\mathbf{R}_\alpha$	t_α^{-1} $(ka = 5.5)$
(0.28, −0.65)	$0.0683 - 0.0160i$
(−0.65, −0.28)	$-0.0658 - 0.0068i$
(0.65, 0.28)	$0.0536 - 0.0341i$
(−0.28, 0.65)	$0.0676 - 0.019\,52i$

elements employed, the scattering directivity is remarkable in our opinion. With the alternative presented here we could design not only finite gratings but also flat lenses, beam splitters, and even cloaking devices. We therefore consider that this work contributes to a direction towards the design of passive devices for the control of mechanic and electromagnetic energy.

ACKNOWLEDGMENTS

A.N.N. acknowledges support from the National Science Foundation through EFRI Grant No. 1641078. P.P. acknowledges support from the National Science Centre in Poland through Grant No. 2018/31/B/ST8/00753. D.T. acknowledges financial support through the "Ramón y Cajal" fellowship under Grant No. RYC-2016-21188 and from the Ministry of Science, Innovation and Universities through Project No. RTI2018- 093921-A-C42.

APPENDIX A: PLATE EQUATIONS AND ENERGY BALANCE

The plate has thickness h, bending stiffness $D[= EI/(1-\nu^2)]$, and density ρ. Time-harmonic motion $e^{-i\omega t}$ is assumed, so that the flexural wave number k is defined by $k^4 = \omega^2\rho h/D$. We assume that there are N point scatterers located at $\mathbf{R}_\alpha$ with impedances t_α, $\alpha = 1, 2, \ldots, N$. The total displacement ψ satisfies

$$D[\Delta^2\psi(\mathbf{r}) - k^4\psi(\mathbf{r})] = \sum_{\alpha=1}^{N} t_\alpha \psi(\mathbf{R}_\alpha)\delta(\mathbf{r}-\mathbf{R}_\alpha). \quad \text{(A1)}$$

A generic attachment impedance t may be modeled as a single degree of freedom with mass M, spring stiffness κ, and damping coefficient ν. Two possible configurations are

$$t = \begin{cases} \left(\dfrac{1}{M\omega^2} - \dfrac{1}{\kappa - i\omega\nu}\right)^{-1}, & \text{case (a)}, \\ M\omega^2 - \kappa + i\omega\nu, & \text{case (b)}. \end{cases} \quad \text{(A2)}$$

In case (a) the mass is attached to the plate by a spring and damper in parallel. Model (b) assumes that the mass is rigidly attached to the plate, and that both are attached to a rigid foundation by the spring and damper in parallel [19]. An important limit is a plate pinned at $\mathbf{R}_\alpha$, $\psi(\mathbf{R}_\alpha) = 0$, which corresponds to $t \to \infty$. The (a) and (b) oscillators could also be attached in parallel, e.g., on either side of the plate, to give $t = t_a + t_b$.

Green's function is the particular solution $\psi = G$ for a single source of the form $\delta(\mathbf{r})$ on the right-hand side of (A1):

$$G(\mathbf{r}) = \frac{i}{8k^2D}[H_0^{(1)}(kr) - H_0^{(1)}(ikr)]. \quad \text{(A3)}$$

The following identity may be found starting from the plate equation (A1) using the procedure of Norris and Vemula [18] for the analogous case without source terms:

$$\operatorname{Im} D \int_{\partial A} [\psi^*(\mathbf{r})\nabla\Delta\psi(\mathbf{r}) - \Delta\psi(\mathbf{r})\nabla\psi^*(\mathbf{r})] \cdot \mathbf{n} ds = \sum_{\alpha=1}^{N} (\operatorname{Im} t_\alpha)|\psi(\mathbf{R}_\alpha)|^2. \quad \text{(A4)}$$

Taking the limit as the bounding surface ∂A tends to infinity, and using Eqs. (1), (11), and (32) yields

$$\operatorname{Im} f(0) = \frac{\int_0^{2\pi} |f(\theta)|^2 d\theta}{16\pi Dk^2} + \sum_{\alpha=1}^{N} (\operatorname{Im} t_\alpha)|\psi(\mathbf{R}_\alpha)|^2. \quad \text{(A5)}$$

Define

$$\sigma_{\text{ext}} = \operatorname{Im} f(0), \quad \text{(A6a)}$$

$$\sigma_{\text{sca}} = \frac{1}{16\pi Dk^2}\int_0^{2\pi} |f(\theta)|^2 d\theta, \quad \text{(A6b)}$$

$$\sigma_{\text{abs}} = \sum_{\alpha=1}^{N} (\operatorname{Im} t_\alpha)|\psi(\mathbf{R}_\alpha)|^2. \quad \text{(A6c)}$$

Then the energy balance becomes

$$\sigma_{\text{ext}} = \sigma_{\text{sca}} + \sigma_{\text{abs}}. \quad \text{(A7)}$$

Note that

$$\sigma_{\text{sca}} = \frac{1}{8Dk^2}\mathbf{A}^{(P)\dagger}\mathbf{A}^{(P)}, \qquad \sigma_{\text{abs}} = \sum_{\alpha=1}^{N} (-\operatorname{Im} t_\alpha^{-1})|B_\alpha^{(P)}|^2, \quad \text{(A8)}$$

where the infinite vector $\mathbf{A}^{(P)}$ and N vector $\mathbf{B}^{(P)}$ are solutions for the passive set of impedances.

A sort of equivalent reasoning can be derived from Eq. (6) by rewriting it in the matrix form

$$\sum_{\alpha=1}^{N} t_\alpha^{-1}|B_\alpha|^2 = \mathbf{B}^\dagger\boldsymbol{\psi}_0 + \mathbf{B}^\dagger\mathbf{G}\mathbf{B}, \quad \text{(A9)}$$

where $\mathbf{G} = \{G(\mathbf{R}_\alpha - \mathbf{R}_\beta)\}$ and $\boldsymbol{\psi}_0 = \{\psi_0(\mathbf{R}_\alpha)\}$. From Eq. (A9) we are interested only in the imaginary part, as it defines the passive or active character of the cluster. Note that the imaginary part of the quadratic form in Eq. (A9) is $\mathbf{B}^\dagger \operatorname{Im}(\mathbf{G})\mathbf{B}$ and $\operatorname{Im}(\mathbf{G}) \propto J_0$; hence, $\operatorname{Im}(\mathbf{G})$ is real valued and symmetric. Finally, for a globally passive cluster, we

require that

$$\sum_{\alpha=1}^{N}(\mathrm{Im}\, t_\alpha^{-1})|B_\alpha|^2 = \mathbf{B}^\dagger \,\mathrm{Im}(\mathbf{G})\mathbf{B} + \frac{1}{2}(\mathbf{B}^\dagger\boldsymbol{\psi}_0 - \mathbf{B}^T\boldsymbol{\psi}_0^*) \le 0. \quad \text{(A10)}$$

Satisfying $\mathrm{Im}\, t_\alpha^{-1} \le 0$ for all individual particles α corresponds to a locally passive metacluster. From Eqs. (A1) and (7), it may be noted that B_α is a complex force amplitude that acts on the plate. The passivity of a single scatterer can be seen through the Poynting vector—characteristic of the direction of energy flow. Time-averaged energy flow through the point at which a scatterer is placed is

$$\Phi = -\tfrac{1}{2}\,\mathrm{Re}(B_\alpha\dot{\psi}_\alpha^\dagger) = \tfrac{1}{2}\omega\psi_\alpha^\dagger\psi_\alpha\,\mathrm{Im}\, t_\alpha, \quad \text{(A11)}$$

where, for $\mathrm{Im}\, t_\alpha \ge 0$, we have $\Phi \ge 0$, so energy flows from the plate towards the scatterer, i.e., the scatterer is passive. Here Φ can be seen as the power absorbed by the scatterer.

APPENDIX B: SOME MATRIX PROPERTIES

It follows from the definition of $\mathbf{S}$ in Eq. (14) and Graf's addition theorem for Bessel functions [see Eq. (9.1.79) of [20]] that $\mathbf{S}^\dagger\mathbf{S}$ simplifies to

$$(\mathbf{S}^\dagger\mathbf{S})_{\alpha\beta} = \sum_{n=-\infty}^{\infty} J_n(kR_\alpha)J_n(kR_\beta)e^{in(\theta_\alpha-\theta_\beta)} = J_0(kR_{\alpha\beta}), \quad \text{(B1)}$$

where $R_{\alpha\beta} = |\mathbf{R}_\alpha - \mathbf{R}_\beta|$. Note that $J_0(kR_{\alpha\beta}) \approx 1$ at low frequency, indicating that $\mathbf{S}^\dagger\mathbf{S}$ becomes singular in this limit. Numerical examples show this in terms of the matrix condition number that becomes large at low frequency.

The $N \times N$ matrix $\mathbf{S}^\dagger\mathbf{S}$ is therefore real, symmetric, and non-negative definite, and can be expressed as

$$\mathbf{S}^\dagger\mathbf{S} = \sum_{\alpha=1}^{N}\lambda_\alpha\mathbf{u}_\alpha\mathbf{u}_\alpha^\dagger \quad \text{(B2)}$$

with positive eigenvalues $\lambda_\alpha > 0$ and normalized eigenvectors of length N, $\mathbf{u}_\alpha^\dagger\mathbf{u}_\beta = \delta_{\alpha\beta}$. Using Eq. (B2) in the definition of $\mathbf{P}$, Eq. (22) yields

$$\mathbf{P} = \sum_{\alpha=1}^{N}\lambda_\alpha^{-1}\mathbf{V}_\alpha\mathbf{V}_\alpha^\dagger, \quad \text{(B3)}$$

where the infinite-dimensional vectors $\mathbf{V}_\alpha$ are

$$\mathbf{V}_\alpha = \mathbf{S}\mathbf{u}_\alpha, \qquad \alpha = 1,\ldots,N. \quad \text{(B4)}$$

These are orthogonal, $\mathbf{V}_\alpha^\dagger\mathbf{V}_\beta = \lambda_\alpha\delta_{\alpha\beta}$, but not orthonormal. We define the orthonormal set

$$\mathbf{U}_\alpha = \lambda_\alpha^{-1/2}\mathbf{S}\mathbf{u}_\alpha, \qquad \alpha = 1,\ldots,N, \quad \text{(B5)}$$

so that $\mathbf{P}$ is in canonical form,

$$\mathbf{P} = \sum_{\alpha=1}^{N}\mathbf{U}_\alpha\mathbf{U}_\alpha^\dagger. \quad \text{(B6)}$$

Hence, $\mathbf{P}$ is finite rank with N nonzero eigenvalues equal to $+1$. Alternatively, $\mathbf{P}$ is a projection onto the N-dimensional subspace $\mathrm{span}\{\mathbf{U}_\alpha,\ \alpha = 1,\ldots,N\}$, and satisfies the projector property

$$\mathbf{P}^2 = \mathbf{P}. \quad \text{(B7)}$$

We note some other properties of $\mathbf{P}$ and related matrices. Multiplying Eq. (22) on the right by $\mathbf{S}$ and on the left by $\mathbf{S}^\dagger$ gives

$$\mathbf{P}\mathbf{S} = \mathbf{S}, \qquad \mathbf{S}^\dagger\mathbf{P} = \mathbf{S}^\dagger. \quad \text{(B8)}$$

The fundamental matrix $\mathbf{S}$ of Eq. (14) has an interesting form in terms of the finite- and infinite-dimensional normalized eigenvectors:

$$\mathbf{S} = \sum_{\alpha=1}^{N}\lambda_\alpha^{1/2}\mathbf{U}_\alpha\mathbf{u}_\alpha^\dagger. \quad \text{(B9)}$$

The Moore-Penrose inverse of $\mathbf{S}$ is

$$(\mathbf{S}^\dagger\mathbf{S})^{-1}\mathbf{S}^\dagger = \sum_{\alpha=1}^{N}\lambda_\alpha^{-1/2}\mathbf{u}_\alpha\mathbf{U}_\alpha^\dagger. \quad \text{(B10)}$$

Similarly, the matrix $\mathbf{Q}$ of Eq. (24) is

$$\mathbf{Q} = \sum_{\alpha=1}^{N}\mathbf{u}_\alpha\mathbf{U}_\alpha^\dagger. \quad \text{(B11)}$$

It follows from this, or from its definition in Eq. (24), that the matrix $\mathbf{Q}$ satisfies

$$\mathbf{Q}^\dagger\mathbf{Q} = \mathbf{P}, \qquad \mathbf{Q}\mathbf{Q}^\dagger = \mathbf{I}_N, \quad \text{(B12)}$$

where $\mathbf{I}_N$ is the identity on $\mathrm{span}\{\mathbf{U}_\alpha,\ \alpha = 1,\ldots,N\}$

Finally, the physical vectors for the far-field pattern function and source strengths of Eqs. (21) and (19) are

respectively

$$\mathbf{A}^{(N)} = \sum_{\alpha=1}^{N} a_\alpha \mathbf{U}_\alpha, \qquad \mathbf{B} = \sum_{\alpha=1}^{N} b_\alpha \mathbf{u}_\alpha, \tag{B13}$$

where

$$a_\alpha = \mathbf{U}_\alpha^\dagger \mathbf{A}, \qquad b_\alpha = \lambda_\alpha^{-1/2} a_\alpha. \tag{B14}$$

[1] Yabin Jin, Bahram Djafari-Rouhani, and Daniel Torrent, Gradient index phononic crystals and metamaterials, Nanophotonics **8**, 685 (2019).

[2] Nader Engheta and Richard W. Ziolkowski, *Metamaterials: Physics and Engineering Explorations* (John Wiley & Sons, Hoboken, 2006).

[3] Pierre A. Deymier, *Acoustic Metamaterials and Phononic Crystals* (Springer Science & Business Media, Heidelberg, 2013), Vol. 173.

[4] Nanfang Yu, Patrice Genevet, Mikhail A. Kats, Francesco Aieta, Jean-Philippe Tetienne, Federico Capasso, and Zeno Gaburro, Light propagation with phase discontinuities: Generalized laws of reflection and refraction, science **334**, 333 (2011).

[5] Alexander V. Kildishev, Alexandra Boltasseva, and Vladimir M. Shalaev, Planar photonics with metasurfaces, Science **339**, 1232009 (2013).

[6] Nanfang Yu and Federico Capasso, Flat optics with designer metasurfaces, Nat. Mater. **13**, 139 (2014).

[7] Younes Ra'di, Dimitrios L. Sounas, and Andrea Alù, Metagratings: Beyond the Limits of Graded Metasurfaces for Wave Front Control, Phys. Rev. Lett. **119**, 067404 (2017).

[8] Alex M. H. Wong and George V. Eleftheriades, Perfect Anomalous Reflection with a Bipartite Huygens? Metasurface, Phys. Rev. X **8**, 011036 (2018).

[9] Daniel Torrent, Acoustic anomalous reflectors based on diffraction grating engineering, Phys. Rev. B **98**, 060101 (2018).

[10] Pawel Packo, Andrew N. Norris, and Daniel Torrent, Inverse Grating Problem: Efficient Design of Anomalous Flexural Wave Reflectors and Refractors, Phys. Rev. Appl. **11**, 014023 (2019).

[11] Vladislav Popov, Fabrice Boust, and Shah Nawaz Burokur, Constructing the near Field and far Field with Reactive Metagratings: Study on the Degrees of Freedom, Phys. Rev. Appl. **11**, 024074 (2019).

[12] Vladislav Popov, Marina Yakovleva, Fabrice Boust, Jean-Luc Pelouard, Fabrice Pardo, and Shah Nawaz Burokur, Designing Metagratings via Local Periodic Approximation: From Microwaves to Infrared, Phys. Rev. Appl. **11**, 044054 (2019).

[13] Yabin Jin, Xinsheng Fang, Yong Li, and Daniel Torrent, Engineered Diffraction Gratings for Acoustic Cloaking, Phys. Rev. Appl. **11**, 011004 (2019).

[14] Huiqin Ni, Xinsheng Fang, Zhilin Hou, Yong Li, and Badreddine Assouar, High-efficiency anomalous splitter by acoustic meta-grating, Phys. Rev. B **100**, 104104 (2019).

[15] Jiajie He, Xue Jiang, Dean Ta, and Weiqi Wang, Experimental demonstration of underwater ultrasound cloaking based on metagrating, Appl. Phys. Lett. **117**, 091901 (2020).

[16] Paul A. Martin, *Multiple Scattering: Interaction of Time-Harmonic Waves with N Obstacles* (Cambridge University Press, Cambridge, 2006), Vol. 107.

[17] Daniel Torrent, Didier Mayou, and José Sánchez-Dehesa, Elastic analog of graphene: Dirac cones and edge states for flexural waves in thin plates, Phys. Rev. B **87**, 115143 (2013).

[18] A. N. Norris and C. Vemula, Scattering of flexural waves on thin plates, J. Sound Vib. **181**, 115 (1995).

[19] D. V. Evans and R. Porter, Penetration of flexural waves through a periodically constrained thin elastic plate in vacuo and floating on water, J. Eng. Math. **58**, 317 (2007).

[20] M. Abramowitz and I. Stegun, *Handbook of Mathematical Functions with Formulas, Graphs, and Mathematical Tables* (Dover, New York, 1974).